



**NIST Technical Note  
NIST TN 2212**

# **Using Monte Carlo Methods to Compute the Uncertainty of Fracture Toughness and Fracture Resistance Curves**

Lucas Koepke  
Timothy S. Weeks  
Jolene Splett

This publication is available free of charge from:  
<https://doi.org/10.6028/NIST.TN.2212>

**NIST Technical Note  
NIST TN 2212**

# **Using Monte Carlo Methods to Compute the Uncertainty of Fracture Toughness and Fracture Resistance Curves**

Lucas Koepke  
*Information Technology Laboratory*

Timothy S. Weeks  
*Material Measurement Laboratory*

Jolene Splett  
*Information Technology Laboratory*

This publication is available free of charge from:  
<https://doi.org/10.6028/NIST.TN.2212>

February 2023



U.S. Department of Commerce  
*Gina M. Raimondo, Secretary*

National Institute of Standards and Technology  
*Laurie E. Locascio, NIST Director and Under Secretary of Commerce for Standards and Technology*

NIST TN 2212  
February 2023

Certain commercial entities, equipment, or materials may be identified in this document in order to describe an experimental procedure or concept adequately. Such identification is not intended to imply recommendation or endorsement by the National Institute of Standards and Technology, nor is it intended to imply that the entities, materials, or equipment are necessarily the best available for the purpose.

### **NIST Technical Series Policies**

[Copyright, Fair Use, and Licensing Statements](#)

[NIST Technical Series Publication Identifier Syntax](#)

### **Publication History**

Approved by the NIST Editorial Review Board on 2022-03-21

### **How to Cite this NIST Technical Series Publication**

Koepke L, Weeks TS, Splett J (2023) Using Monte Carlo Methods to Compute the Uncertainty of Fracture Toughness and Fracture Resistance Curves. (National Institute of Standards and Technology, Gaithersburg, MD), NIST Technical Note (TN) NIST TN 2212. <https://doi.org/10.6028/NIST.TN.2212>

### **NIST Author ORCID iDs**

Timothy S. Weeks: 0000-0001-8553-2505

## **Abstract**

The uncertainty of fracture toughness and associated fracture resistance curves for single edge-notched tension (SE(T) or SENT) specimens is a key component missing from widely accepted testing protocols. Complicating matters, these uncertainties are not easily calculated using traditional propagation-of-error techniques. Uncertainty estimation using Monte Carlo techniques for two test methods are presented and the effect of changing the distribution and tolerance specified for the measurement and input quantities on the results is investigated.

## **Key words**

Crack tip opening displacement; CTOD; CTOD-R; Fracture resistance; fracture resistance curve; fracture toughness;  $J$ -integral;  $J$ -R; Monte Carlo methods; propagation of errors; experimental error; SENT; SE(T); single-edge-notched tension; uncertainty.

## Table of Contents

<b>1. Introduction</b> .....	<b>1</b>
<b>2. Measurement Procedure</b> .....	<b>1</b>
<b>3. Analysis Methods</b> .....	<b>4</b>
<b>4. Monte Carlo Simulation</b> .....	<b>9</b>
<b>5. Intermediate Calculations</b> .....	<b>11</b>
5.1. CTOD-R Method Calculations .....	12
5.2. J-R Method Calculations .....	15
<b>6. Monte Carlo Results</b> .....	<b>18</b>
6.1. CTOD-R Results .....	20
6.2. J-R Results.....	21
<b>7. Discussion</b> .....	<b>22</b>
<b>8. Conclusions</b> .....	<b>23</b>
<b>References</b> .....	<b>24</b>

## List of Tables

Table 1. Pre-test specimen geometry measurement tolerances (all units in mm).....	3
Table 2. Coefficients $r_k$ in Eq. (1).....	4
Table 3. Values of $\tau_k$ to be used in Eq. (6).....	6
Table 4. Values of $\varphi_k$ to be used in Eq. (8).....	7
Table 5. Values of $\psi_k$ to be used in Eq. (9).....	7
Table 6. Measurement tolerances on acquired data.....	10
Table 7. Resulting $a_{0q}$ and power law fitting coefficients for the two methods and different data distributions.....	19

## List of Figures

Figure 1. (a) Notch geometry and integral knife-edge details for fatigue pre-cracked specimens, (b) details of the side grooves for each specimen, [the total reduction in thickness is $0.15B$ ], (c) and double-clip-gauge mounting and height details. (All linear dimensions are in mm).....	3
Figure 2. Plot of force vs. calculated $\delta_M$ for the CTOD-R method (black) and observed CMOD for the J-R method (red), noting very little discernable difference in the source data. The circle data points denote the force associated with each $j^{th}$ -cycle and the one solid circle data point denotes the cycle with the maximum load ( $P_u$ ); this unloading (19) is used later.	12
Figure 3. (a) Observed $\delta_M$ vs force from unloading 19. (b)-(d) Simulated data for unloading 19 based on three candidate distributions and the measurement tolerances specified in Table 1 and Table 6.....	13

Figure 4. Data and fitted curves to obtain  $a_{0q}$  for (a) observed  $\delta_M$  vs calculated  $a_j$  data and for (b)-(d) simulated data for three candidate distributions based on the measurement tolerances specified in Table 1 and Table 6..... 14

Figure 5. Data and fitted CTOD-R curves for (a) observed CTOD-R data and for (b)-(d) simulated data for three candidate distributions based on the measurement tolerances specified in Table 1 and Table 6..... 15

Figure 6. (a) Observed data for the *J-R* method, unloading 19. (b)-(d) Simulated data for unloading 19 based on three candidate distributions and the measurement tolerances specified in Table 1 and Table 6..... 16

Figure 7. Data and fitted curves to obtain  $a_{0q}$  for (a) observed *J-R* data and for (b)-(d) simulated data for three candidate distributions based on the measurement tolerances specified in Table 1 and Table 6..... 17

Figure 8. Data and fitted *J-R* curves for (a) observed *J-R* method data and for (b)-(d) simulated data for three candidate distributions based on the measurement tolerances specified in Table 1 and Table 6..... 18

Figure 9. Estimated CTOD-R curves for observed data (black lines) and 95 % coverage bands estimated via simulation (gray shaded regions); (a)-(b) simulations with a normal distribution based on the full tolerance and on 50 % of the measurement tolerances specified in Table 1 and Table 6, (c)-(d) for a uniform distribution, (e)-(f) for a triangular distribution..... 20

Figure 10. Estimated *J-R* curves for observed data (black lines) and 95 % coverage bands estimated via simulation (gray shaded regions). (a)-(b) simulations with a normal distribution based on the full tolerance and on 50 % of the measurement tolerances specified in Table 1 and Table 6, (c)-(d) for a uniform distribution, (e)-(f) for a triangular distribution. .... 21

## 1. Introduction

Determining the fracture toughness and fracture resistance curves of metallic materials is a complicated process, and several test methods are available to describe the test procedure and associated computations [1-5]. None of these methods, however, provide guidance to estimate the uncertainty of the final measurement results. Because of the complex nature of the test procedure and computations, traditional propagation-of-errors techniques found in Ref. [6] are not practical. The purpose of this paper is to demonstrate that the uncertainty of the predicted starting crack depth,  $a_{0q}$ , and the fitting parameters of the J-integral or crack tip opening displacement (CTOD) resistance curves can be obtained using Monte Carlo simulations according to Ref. [7]. Methods of analyzing the measurement data for CTOD-R curves are outlined in the test protocol published by ExxonMobil Upstream Research Company [3]. Methods of analyzing the measurement data for  $J$ -R curves are outlined in the recommended practice published by Natural Resources Canada – CanmetMATERIALS [2]. The methods to determine CTOD-R and  $J$ -R curves were developed independently and for different technical reasons. Since their original publication, many research programs have endeavored to improve and expand the methods and applicability. The background and evolution of the methods is outside the scope of this work. While giving credit to the originating authors and organizations that developed the framework for the methods, the methods have evolved sufficiently in time to be generally referred to as the CTOD-R and  $J$ -R methods.

Multiple industrial and standards development organizations have endeavored to standardize the test protocols with varying degrees of success and completion. One of the challenges to standardizing the test and analysis methods is ensuring that measurement uncertainty can be estimated. This work further demonstrates that Monte Carlo methods can be employed on many other complex test and analysis methods. Various levels of tolerance associated with input and measurement quantities are investigated as well as three possible distributions for those uncertainties.

## 2. Measurement Procedure

The clamped single edge-notched tension (SE(T) or SENT) specimen has been widely used in a single-specimen testing scheme to generate fracture resistance curves. The SE(T) specimen with appropriate notch geometry is a low-constraint specimen designed to reduce conservatism in the measurement of fracture toughness. The crack driving force is taken as either the  $J$ -integral or CTOD. The CTOD-R method uses a double-clip-gauge configuration where two clip gauges measure the crack opening displacement (COD, denoted by  $V$ ), at two different distances ( $h_1$  and  $h_2$ ) from the surface of the specimen. Using the two measurements and the known distances, the crack mouth opening displacement (CMOD) is calculated at the surface of the specimen. In contrast the  $J$ -R method uses a single clip gauge attached at the surface of the specimen to measure the CMOD directly. The minimum test record for the CTOD-R method will include the COD at  $h_1$  ( $V_1$ ), and the COD at  $h_2$  ( $V_2$ ), in addition to force. The minimum test record for the  $J$ -R method will include CMOD and force. Both test procedures use the same specimen geometry, gripping and loading

conditions. Both test procedures use a CMOD unloading compliance (UC) method to determine the change in crack length. The results of a direct comparison experiment were published by Weeks and Lucon [8], where the CTOD-R and  $J$ -R methods were employed during the same test. Barring minor differences in some of the procedural details and end-of-test conditions, the recommended practices were followed closely. Likewise, the analysis procedures as detailed in each recommended practice were followed closely in this work. One relevant difference is the end-of-test condition; this is specified in the CTOD-R procedure to determine the final crack length from an unloading compliance without significant plastic deformation. The end-of-test condition is simply taken as an unloading that follows the maximum force ( $P_U$ ) during the test but does not exceed a  $0.2P_U$  drop in load at the beginning of the unloading portion. This is to avoid significant plastic necking that influences the crack growth estimate. No such end-of-test condition is described in the  $J$ -R procedure source documents. For the purposes here, the end-of-test condition as prescribed in the CTOD-R procedure is used for both methods.

Pre-test measurements of specimen and fixture geometry are given according to Fig. 1. In this work, only a square cross-section ( $W = B, B \times W$ ) specimen is considered. However, the measurement uncertainty and the propagated influence is expected to be very small if alternate ( $B \times 2B$ ) geometries are considered. The clamped specimen has a minimum “daylight” between fixed hydraulic grips of  $10W$ . Few measurement methods are prescribed in either of the test procedures, and in general, any method that has enough resolution and can be repeated should be adequate. These methods through the course of pre-test measurements and post-test measurements may include calipers, comparators, microscopes, or any combination, but not exclusive of other methods such as a coordinate measurement machine (CMM) or a profilometer. Digital equipment that includes a recording method (such as having a statistical process control output) are preferred to a manually read and recorded measurement to avoid reading and transcription errors.

For each of the pre-test specimen dimensions, the procedures provide either explicit or implicit measurement tolerances; these conditions imply a minimum resolution and are given in Table 1. The implicit limits are assumed from other measurement standards that the procedures considered here have referenced. In all instances, the tolerances provided herein include the uncertainty of the measurement instrument/method considered.

The initial crack length ( $a_0$ ) will always be determined from post-test measurements, whether the specimen is fatigue pre-cracked or not. In situ measurements during the test may include  $COD_1$  and  $COD_2$  ( $V_1$  and  $V_2$ ) and force ( $P$ ), or CMOD and force ( $P$ ) as applicable. The measurement tolerances for clip gauge and force measurements are given implicitly by the applicable calibration standards.

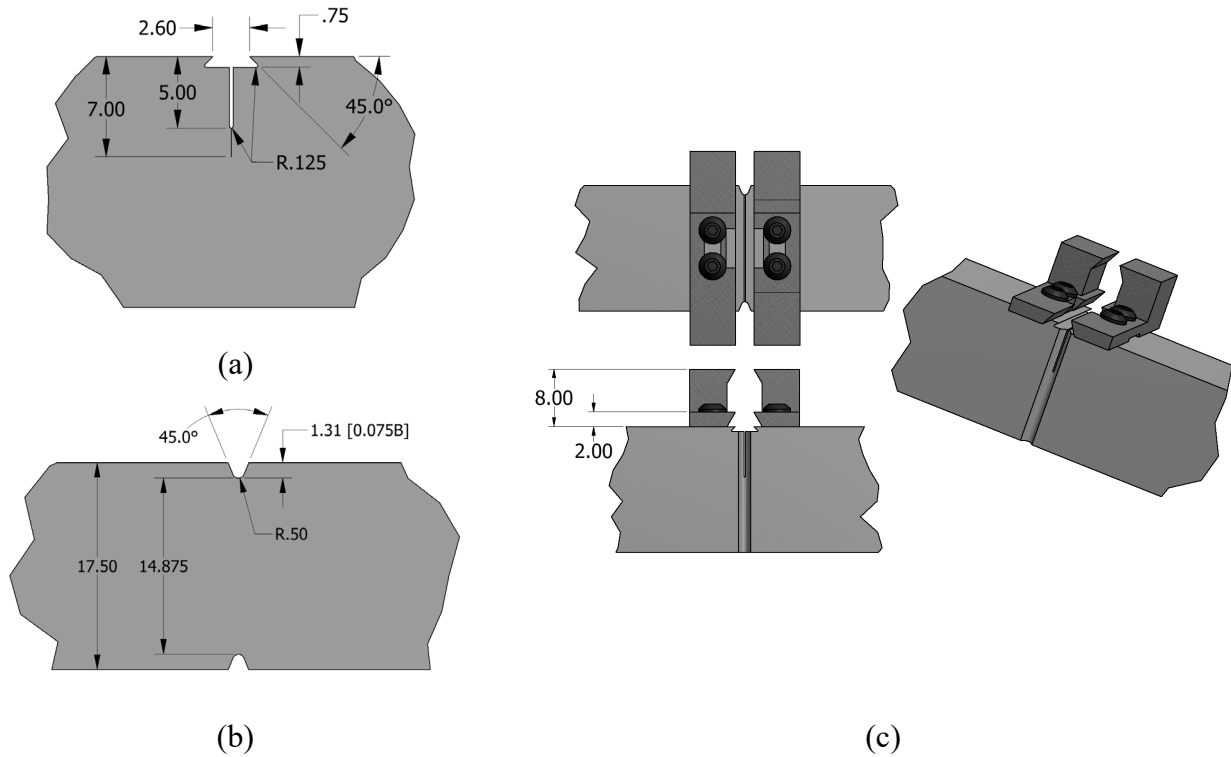


Figure 1. (a) Notch geometry and integral knife-edge details for fatigue pre-cracked specimens, (b) details of the side grooves for each specimen, [the total reduction in thickness is  $0.15B$ ], (c) and double-clip-gauge mounting and height details. (All linear dimensions are in mm).

Table 1. Pre-test specimen geometry measurement tolerances (all units in mm)

Measurement	CTOD-R Method	<i>J</i> -R Method
<i>B</i>	0.050 ( <b>0.5 %</b> )	0.050 ( <b>0.5 %</b> )
<i>B<sub>N</sub></i>	0.050 ( <b>0.5 %</b> )	0.050 ( <b>0.5 %</b> )
<i>W</i>	0.050 ( <b>0.5 %</b> )	0.050 ( <b>0.5 %</b> )
<i>h</i> <sub>1</sub>	0.2 %	n/a
<i>h</i> <sub>2</sub>	0.2 %	n/a

*Note: where a secondary tolerance is shown in parentheses, the larger of the two tolerances should be used. The bolded value represents the limit used in this study.*

### 3. Analysis Methods

The computations outlined in the procedures take the measured force and displacement data and produce two outputs: the change in crack length ( $\Delta a$ ) and the crack driving force as defined by the CTOD or  $J$ -integral. Since these computations involve multiple complicated steps, both the CTOD-R and  $J$ -R calculations are summarized here.

For both methods, the crack depth  $a_j$  is first calculated for each of the unloading/loading cycles (each cycle is denoted numerically as  $j$ ) from the compliance of the unloading portion of the data set for each cycle.

The CTOD-R method uses a 5<sup>th</sup> order polynomial to determine  $a_j$  whereas the  $J$ -R method uses a 9<sup>th</sup> order polynomial equation. Both methods use the form found in Eq. (1), where  $n = 5$ , and  $n = 9$  correspond to the CTOD-R, and  $J$ -R methods respectively. The coefficients for the polynomials can be found in Table 2.

$$\frac{a_j}{W} = \sum_{k=0}^n r_k U_j^k \quad (1)$$

Table 2. Coefficients  $r_k$  in Eq. (1).

$k$	CTOD-R Method	$J$ -R Method
0	1.64461	2.044
1	-8.7084	-15.732
2	30.31342	73.238
3	-69.60922	-182.898
4	83.52325	175.653
5	-39.11201	60.930
6		-113.997
7		-113.031
8		8.548
9		142.840

The term  $U_j$  in Eq. (1) is the normalized unloading compliance for each of the unloading/loading cycles. The unloading compliance is calculated differently between the two methods. The CTOD-R method must first convert the crack opening displacements ( $V_1$  and  $V_2$ ) to crack mouth opening displacement (CMOD ( $\delta_M$ )) by way of Eq. (2). The  $J$ -R method measures CMOD directly and is available in the raw data record.

$$\delta_M = V_1 - \frac{h_1}{h_2 - h_1} (V_2 - V_1) \quad (2)$$

Equation 3 is used to determine the normalized unloading compliance for the CTOD-R method,

$$U_j = \frac{1}{1 + \sqrt{B_{eff} C_{\delta_M(j)} E'}}$$

where,

$$\begin{aligned} C_{\delta_M(fj)} &= (\Delta\delta_M/\Delta P)_j \\ B_{eff} &= B - (B - B_N)^2/B, \text{ and} \\ E' &= E/(1 - \nu^2). \end{aligned} \tag{3}$$

The *J*-R method uses a similar equation (see Eq. (4)) to determine the normalized unloading compliance but it includes a correction method that accounts for plastic necking and specimen rotation:

$$U_j = \frac{1}{1 + \sqrt{B_{eff} C_{corr(j)} E}}$$

where,

$$\begin{aligned} C_{corr(fj)} &= (\Delta C_{MOD}/\Delta P)_j / F_j \\ B_{eff} &= B - (B - B_N)^2/B \\ F_j &= 1 - 0.165 \frac{a_0 P_j}{W P_Y'}, \text{ and} \\ P_Y &= \sigma_Y B_N (W - a_0). \end{aligned} \tag{4}$$

The CTOD-R method requires that CTOD be calculated according to Eq. (5).

$$\delta = V_1 - \frac{h_1 + a_0}{h_2 - h_1} (V_2 - V_1) \tag{5}$$

The  $J$ -R method is more computationally complicated and uses the following equations,

$$J_j = \frac{(K_j)^2(1 - \nu)^2}{E} + J_{pl(j)}$$

where,

$$K_j = \left[ \frac{P_j \sqrt{\pi a_j}}{W \sqrt{B B_N}} \right] G \left( \frac{a_j}{W} \right) \quad (6)$$

$$B_{eff} = B - (B - B_N)^2 / B, \text{ and}$$

$$G \left( \frac{a_j}{W} \right) = \sum_{k=1}^{12} \tau_k \left( \frac{a_j}{W} \right)^{k-1},$$

and the parameters  $\tau_k$  are listed in Table 3.

Table 3. Values of  $\tau_k$  to be used in Eq. (6)

$k$	1	2	3	4	5	6
$\tau_k$	1.197	-2.133	23.886	-69.051	100.462	-41.397
$k$	7	8	9	10	11	12
$\tau_k$	-36.137	51.215	-6.607	-52.322	18.574	19.465

The value of the plastic part of the  $J$ -integral ( $J_{pl(j)}$ ) is given by

$$J_{pl(j)} = \left[ J_{pl(j-1)} \left( \frac{\eta_{CMOD(j-1)}}{W - a_{j-1}} \right) \left( \frac{A_{pl(j)} - A_{pl(j-1)}}{B_N} \right) \right] \left[ 1 - \frac{\gamma_{LLD(j-1)}(a_j - a_{j-1})}{W - a_{j-1}} \right] \quad (7)$$

where  $\eta_{CMOD(j-1)}$  and  $\gamma_{LLD(j-1)}$  are evaluated from Eq. (8) and Eq. (9) respectively.

$$\eta_{CMOD(j-1)} = \sum_{k=0}^{10} \varphi_k \left( \frac{a_j}{W} \right)^k \quad (8)$$

using the parameters  $\varphi_k$  listed in Table 4.

Table 4. Values of  $\varphi_k$  to be used in Eq. (8)

$k$	0	1	2	3	4	
$\varphi_k$	1.000	-1.089	9.519	-48.572	109.225	
$k$	5	6	7	8	9	10
$\varphi_k$	-73.116	-77.984	38.487	101.401	43.306	-110.770

Next  $\gamma_{LLD(j)}$  is calculated using the formula

$$\gamma_{LLD(j)} = \eta_{LLD(j)} - 1 - \left(1 - \frac{a_j}{W}\right) \frac{\eta'_{LLD(j)}}{\eta_{LLD(j)}}$$

where,

$$\eta'_{LLD(j)} = \sum_{k=0}^{10} k \psi_k \left(\frac{a_j}{W}\right)^{k-1}, \text{ and} \tag{9}$$

$$\eta_{LLD(j)} = \sum_{k=0}^{10} \psi_k \left(\frac{a_j}{W}\right)^k$$

and the parameters  $\psi_k$  are listed in Table 5.

Table 5. Values of  $\psi_k$  to be used in Eq. (9)

$k$	0	1	2	3	4	
$\psi_k$	-0.880	15.90	-35.440	18.644	18.399	
$k$	5	6	7	8	9	10
$\psi_k$	-1.2373	-12.756	-12.202	-4.447	5.397	14.187

Finally,  $A_{pl(j)}$  is calculated according to Eq. (10).

$$A_{pl(j)} = A_{pl(j-1)} [P_j + P_{j-1}] (CMOD_{pl(j)} - CMOD_{pl(j-1)}) / 2 \quad (10)$$

where,

$$CMOD_{pl(j)} = CMOD_j - (P_j C_{CMOD(j)}).$$

The initial crack length  $a_{0q}$  is estimated next as this value is required for the fracture resistance curves. In the CTOD-R method,  $a_{0q}$  is estimated by fitting the crack depth versus CTOD ( $\delta_j$ ) (see Eq. (7) of [3]) using

$$a_j = a_{0q} + \frac{\delta_j}{1.4} + C_1 \delta_j^2 + C_2 \delta_j^3. \quad (11)$$

The range of data for fitting the model in Eq. (11) is  $\min(a_j)$  to the final crack depth (see 9.3.2 and Fig. 13 in [3]).

In the  $J$ -R method, the crack depth  $a_j$  versus  $J_j$  is used to estimate  $a_{0q}$  (see Eq. (14) of [2]) according to the following equation

$$a_j = a_{0q} + \frac{J_j}{2\sigma_Y} + B_1 J_j^2 + B_2 J_j^3 + \epsilon_j \quad (12)$$

where  $\sigma_Y$  is the material's yield strength. The range of data used for fitting the model in Eq. (12) is from  $\min(a_j)$  to the unloading that occurs immediately before the maximum load. The upper limit is not the end-of-test condition for the  $J$ -R method, instead, it is the fitting boundary condition to determine  $a_{0q}$ , similar to the method described in ASTM E1820 - Standard Test Method for Measurement of Fracture Toughness [1]. Using  $\min(a_j)$  ameliorates the problem of non-physical apparent negative crack growth. The goal of both methods is to estimate  $a_{0q}$ , which is then used to compute crack growth,  $\Delta a_j$ , for each unloading/loading cycle using  $\Delta a_j = a_j - a_{0q}$ .

Finally, the resistance curves are plotted using CTOD, or  $J$ , vs  $\Delta a_j$ . Fitting parameters of the CTOD-R or  $J$ -R curves are determined from Eq. (13) and Eq. (14) given below. The power law fitting parameters ( $\alpha_\delta$  and  $\eta_\delta$ ) for the CTOD-R curve are determined from (Eq. (9) in [3])

$$CTOD = \alpha_\delta (\Delta a)^{\eta_\delta}. \quad (13)$$

The range of data for the CTOD-R fit is from  $\Delta a_j = 0.5$  mm to the last measured crack growth value (see 9.3.5 and Fig. 15 in [3]) using the method of least squares.

The model for the  $J$ -R curve is not specified in the  $J$ -R method source documents yet it is frequently fit to a power law equation just as the CTOD-R curve is fit. This is consistent with other  $J$ -R test standards with different geometries, so the power law model (Eq. (A9.7) from [1]) is used to determine the parameters ( $\alpha_J$  and  $\eta_J$ ),

$$J = \alpha_J (\Delta a)^{\eta_J} + \epsilon_j. \quad (14)$$

The range of data for the  $J$ -R fit is not specified in the source documents, so the fitting range will be set to match that of the CTOD-R method.

Fitting the CTOD-R and  $J$ -R curves requires the use of nonlinear least squares (NLS) since the exponent is estimated as one of the parameters. NLS can be sensitive to the starting values, and occasionally does not converge to a solution.

#### 4. Monte Carlo Simulation

The complex nature of the calculations described in Sec. 3 is not conducive to uncertainty estimation using propagation-of-errors techniques. Instead, a Monte Carlo approach as described in GUM Supplement I [7] is used to obtain uncertainty estimates of  $a_{0q}$  and the parameters of the CTOD-R ( $\hat{\alpha}_\delta$ ,  $\hat{\eta}_\delta$ ) and  $J$ -R ( $\hat{\alpha}_J$ ,  $\hat{\eta}_J$ ) curves. The steps of this Monte Carlo algorithm are as follows:

1. Specify distributions and associated parameters for each input quantity based on available data.
2. Generate random perturbations of each observed data point according to the parameters of step 1.
3. Compute  $\hat{a}_{0q}$  and ( $\hat{\alpha}_\delta$ ,  $\hat{\eta}_\delta$ ) or ( $\hat{\alpha}_J$ ,  $\hat{\eta}_J$ ) as appropriate using the perturbed data set.
4. Discard samples where the calculations failed, or where  $\hat{a}_{0q}$  differs from initial crack length,  $a_0$ , by more than 0.5 mm.

5. Repeat steps 2 to 4 many times and build simulated distributions of the quantities of interest.
6. Compute the standard uncertainty and coverage interval for each of the simulated distributions.

Table 6 lists measurement tolerances for in-situ measured quantities for the two test methods. Not all measurement tolerances are quantified in the two standards. For example, coefficients obtained by finite element analysis for the *J*-R method (see Tables 2-4 of [2]) are provided without uncertainties or tolerances.

Table 6. Measurement tolerances on acquired data

Measurement	CTOD-R Method	<i>J</i> -R Method
$P$ (N)	0.2 %	0.2 %
<i>CMOD</i> (mm)	n/a	0.2 %
$V_1$ (mm)	0.2 %	n/a
$V_2$ (mm)	0.2 %	n/a

*Note: Pre-test specimen geometry measurement tolerances are shown in Table 1.*

The measurement tolerances in Table 1 and Table 6 can either be bounds on the value of an input quantity or actual uncertainties of a measurand. For example, the tolerance prescribes that the value of an input must be known within a range of values or that input has a known uncertainty associated with it. The latter is usually known from calibrations or statistical process data. The distributions associated with the tolerances are not declared in the source documents of either method, so the following analysis considers three reasonable options:

- Specifications are bounds to uniform distributions.
- Specifications are bounds to triangular distributions.
- Specifications are uncertainties associated with normal distributions.

For example, the input quantity for the specimen thickness,  $B$ , has a tolerance of  $\pm 0.050$  mm, and without specific guidance the distribution of  $B$  is either uniform or triangular on the interval  $[B - 0.050 \text{ mm}, B + 0.050 \text{ mm}]$ , or can be assumed to be a normal distribution with mean  $B$  and standard deviation of 0.025 mm (setting the standard deviation as half of the tolerance produces a distribution where approximately 95 % of the sampled values will be between  $B - 0.050$  mm and  $B + 0.050$  mm). A simulated value of  $B$  is obtained by generating a random draw from the chosen distribution.

All code used to analyze the data in this document is written using R [9]. For each combination of method (CTOD-R or *J*-R) and distribution (uniform, triangular, or normal) the objective is to obtain 10,000 valid data sets. A single simulated data set can fail to produce valid results if  $\hat{a}_{0q} > \min(\hat{a}_j)$  in the region of interest, if any of the intermediate NLS fits fail, or if the CTOD-R or *J*-R curve is convex instead of concave. Such data sets are discarded, and a new data

set is obtained. The next section does a deep dive into the intermediate calculations for each method, offering an illuminating view into both methods. The results from the Monte Carlo simulation are shown in Sec. 6.

## 5. Intermediate Calculations

This section illustrates the computation process, using both methods, to determine  $a_{0q}$ , and CTOD-R or  $J$ -R curve parameters from observed data. While the equations and steps have been previously presented, this section is critical to understanding how adding the tolerances from Table 1 and Table 6 affects all the calculations. The observed data used in this paper is shown in Fig. 2. The data and analysis were previously published in Ref. [8] as specimen HT-105-10. The specimen measurements are  $B = 17.529$  mm,  $B_N = 14.928$  mm,  $W = 17.529$  mm,  $h_1 = 2.000$  mm,  $h_2 = 8.000$  mm, and  $a_0 = 6.978$  mm. Post-test measurement of  $a_0$  is based on the 9-point method with a tolerance of 0.025 mm. The material properties necessary for the calculations include  $\sigma_Y = 745$  MPa,  $\nu = 0.3$  (ul), and  $E = 205$  GPa. The intention of this work is to determine measurement-specific influences on the uncertainty separate from material-properties-related uncertainty, therefore, the uncertainty in the material properties for the purposes here is set to zero. For each distribution (normal, uniform, and triangular), data is simulated based on the tolerances in Table 1 and Table 6 to perform the necessary intermediate calculations.

To provide insight into the intermediate calculations, the analyses for the CTOD-R method will be followed by the  $J$ -R method, before showing the Monte Carlo results. Plots are presented of observed data from a single unloading, the calculated data used to estimate  $a_{0q}$ , and the CTOD-R or  $J$ -R curves as well as the fit as appropriate for each method. Results are shown for simulated data sets based on the three assumed distributions and the uncertainty specifications in Table 1 and Table 6. Again, the goal is to illustrate the effect of each choice on the intermediate calculations and the result.

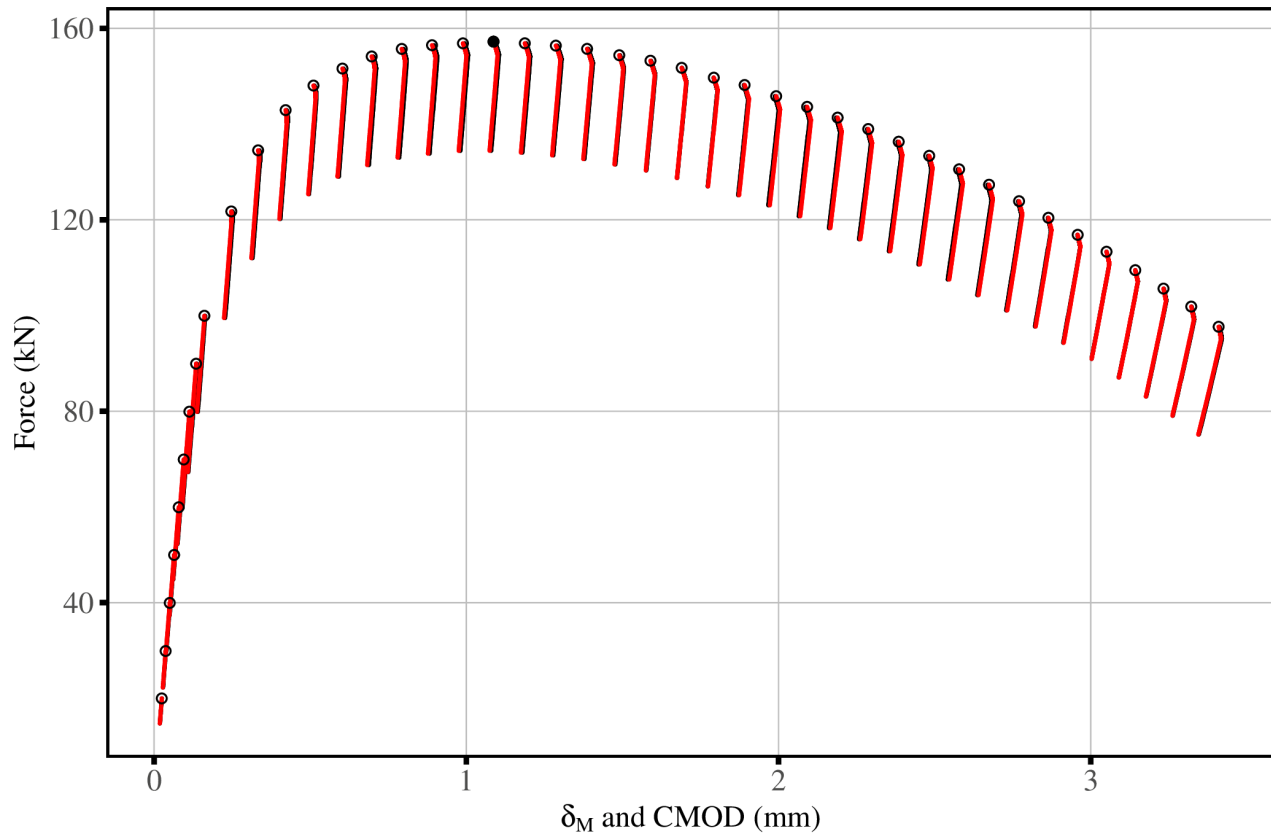


Figure 2. Plot of force vs. calculated  $\delta_M$  for the CTOD-R method (black) and observed CMOD for the *J*-R method (red), noting very little discernable difference in the source data. The circle data points denote the force associated with each  $j^{\text{th}}$ -cycle and the one solid circle data point denotes the cycle with the maximum load ( $P_u$ ); this unloading (19) is used later.

### 5.1. CTOD-R Method Calculations

Unloading number 19 from the observed data is used here to illustrate the effects of distributional assumptions and uncertainty specifications on the simulated data. The observed data is shown in Fig. 3a. Figs. 3b-3d display simulated data based on normal, uniform, and triangular distributions and the uncertainty specifications in Table 1 and Table 6. The variability in all three simulated data sets is much larger than the variability in the observed data. Although the general features remain with respect to the “relaxation” and intentional unloading (in displacement control) none of the simulated data retain the distinct elbow and the tight correlation between adjacent points. Whether the specified tolerances produce realistic data is an unanswered question, but that is of significant interest.

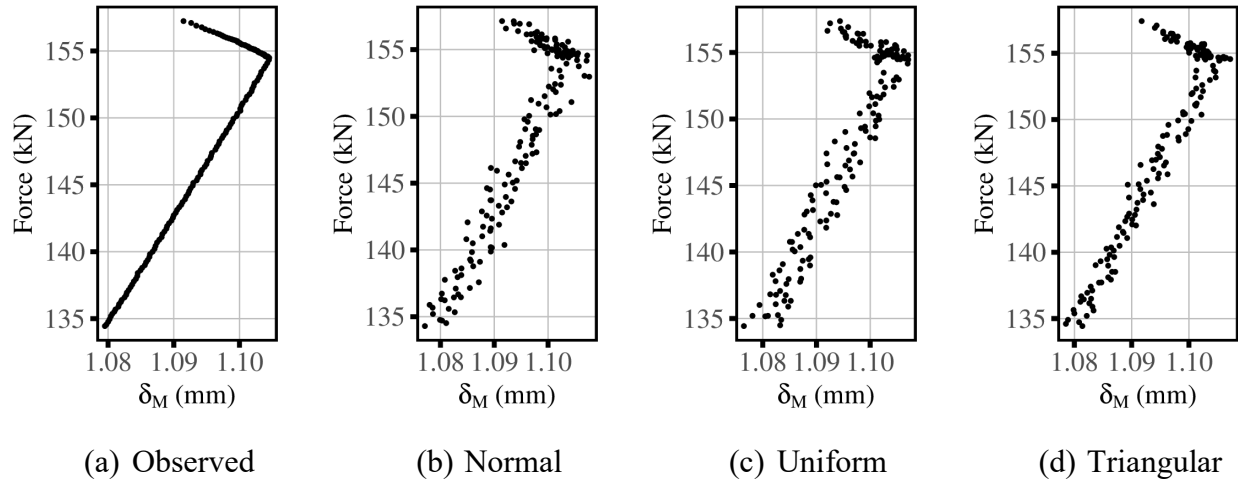


Figure 3. (a) Observed  $\delta_M$  vs force from unloading 19. (b)-(d) Simulated data for unloading 19 based on three candidate distributions and the measurement tolerances specified in Table 1 and Table 6.

The next step in the analysis after generating the simulated data sets is to estimate  $a_{0q}$ . Calculations of  $a_j$  for each loading are completed next. Continuing with the side-by-side comparison of observed data and simulated data, Fig. 4a shows  $a_j$  and CTOD ( $\delta_j$ ) values used in the  $a_{0q}$  fit for the observed data, while Figs. 4b-4d show the fits based on  $a_j$  and  $\delta_j$  values calculated from the simulated data for each of the three distributions of interest. The variability of the observed data about the fitted curve is very small compared to the variability of the simulated data sets about their fitted curves.

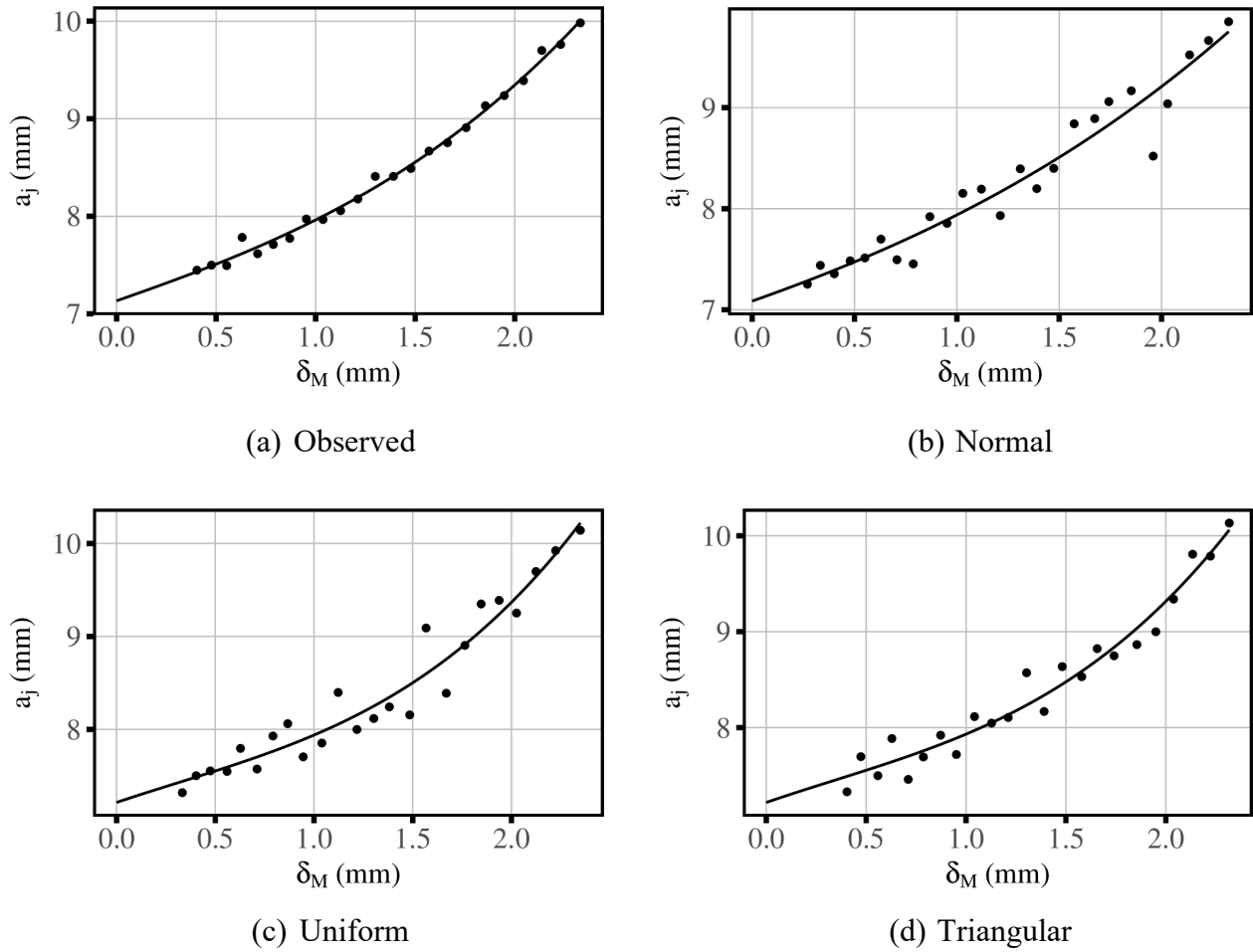


Figure 4. Data and fitted curves to obtain  $a_{0q}$  for (a) observed  $\delta_M$  vs calculated  $a_j$  data and for (b)-(d) simulated data for three candidate distributions based on the measurement tolerances specified in Table 1 and Table 6.

The last step in the CTOD-R method is to fit the CTOD-R curve. The fitted curves, and the data used for those fits, are shown in Fig. 5a for the observed data, and Figs. 5b-5d for the simulated data. As with the  $a_{0q}$  fits, the CTOD-R curve fit shows noticeably better fit for the observed data than for the simulated data.

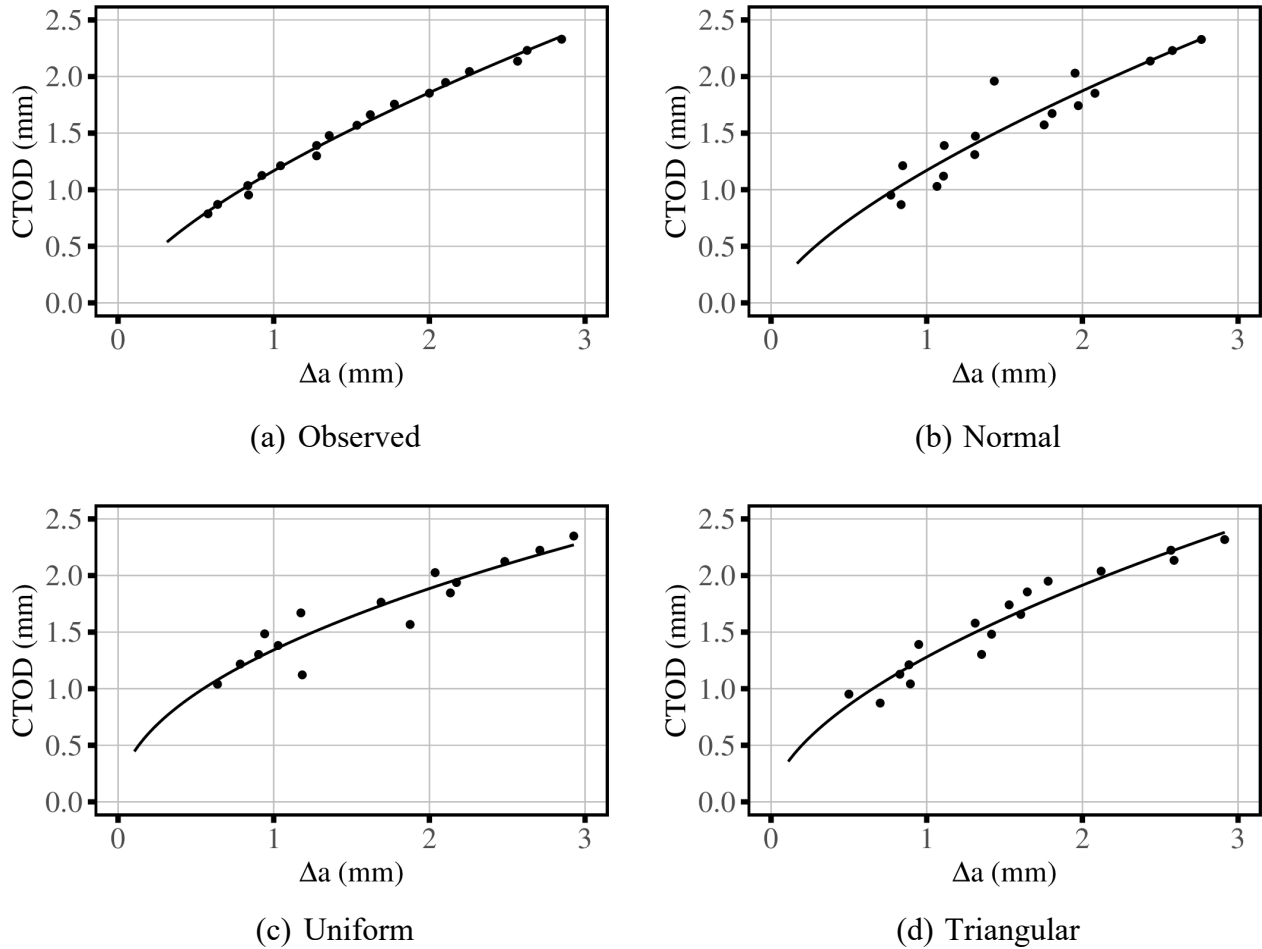


Figure 5. Data and fitted CTOD-R curves for (a) observed CTOD-R data and for (b)-(d) simulated data for three candidate distributions based on the measurement tolerances specified in Table 1 and Table 6.

## 5.2. J-R Method Calculations

A similar approach to that of Sec. 5.1 is used to illustrate the *J-R* method, stepping through the calculations, and comparing the observed data to simulated data for the three distributions of interest. The observed data for unloading number 19 is shown in Fig. 6a, and in Figs. 6b-6d for simulated data. Just as for the CTOD-R method, the observed data shows sharply defined features of relaxation preceding the subsequent intentional unloading points. These features are again much less defined for the simulated data sets.

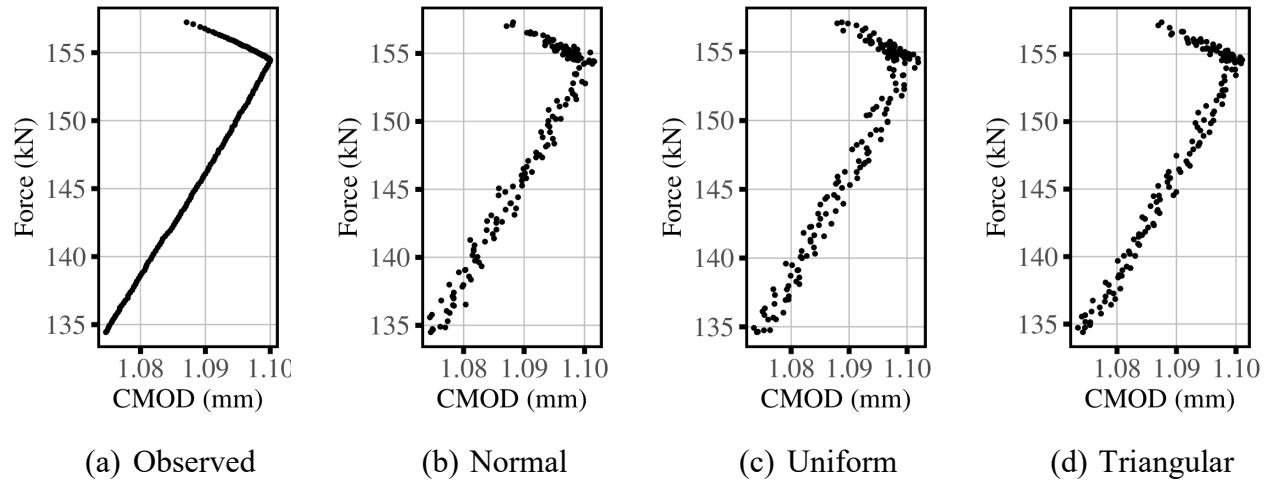


Figure 6. (a) Observed data for the  $J$ -R method, unloading 19. (b)-(d) Simulated data for unloading 19 based on three candidate distributions and the measurement tolerances specified in Table 1 and Table 6.

Figure 7 shows the crack length vs.  $J$  as well as the cubic curve fits to obtain the estimate of  $a_{0q}$ . Although both the CTOD-R and  $J$ -R methods use a cubic function to calculate  $a_{0q}$ , there is more variability in the curve shapes for the  $J$ -R method, possibly due to different criteria for which points are used in the fit. The observed data and fit are shown in Fig. 7a. For the observed data, the fitted curve appears to give a reasonable value when extrapolated to  $J = \text{zero}$ , giving the estimated  $a_{0q}$ . The simulated data and fits are shown in Figs. 7b-7d for each distribution, respectively. The increased variability in the simulated data sets is expected to influence the  $a_{0q}$  estimates.

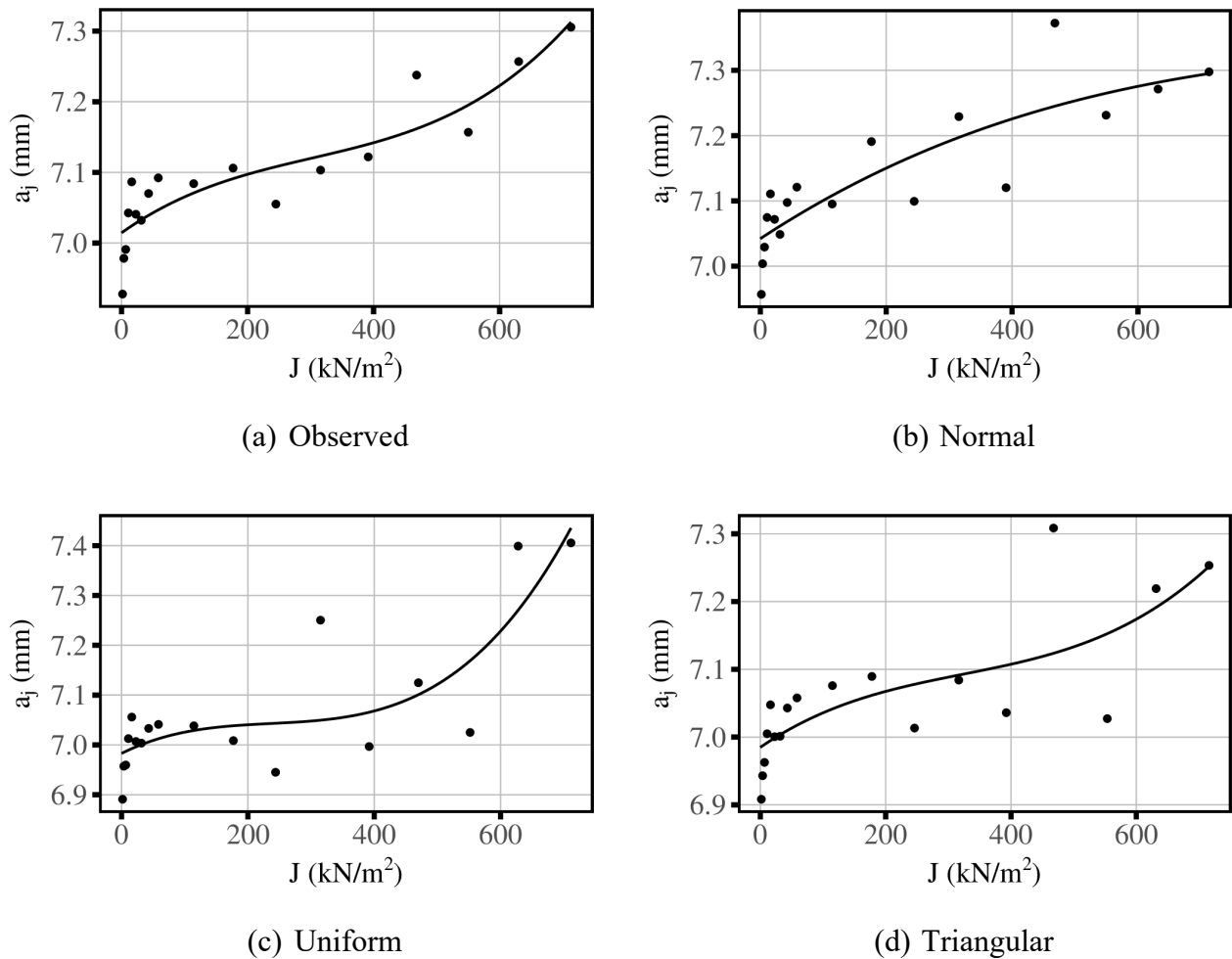


Figure 7. Data and fitted curves to obtain  $a_{0q}$  for (a) observed  $J$ - $R$  data and for (b)-(d) simulated data for three candidate distributions based on the measurement tolerances specified in Table 1 and Table 6.

The results of fitting the  $J$ - $R$  curves are shown in Fig. 8a for the observed data, and in Figs. 8b-d for simulated data. For the observed data, the estimated  $J$ - $R$  curve appears to adequately represent the data. For the three simulated data sets, and especially for the data based on the normal distribution, the amount of variability in the data is larger. A residual analysis is necessary to determine the goodness of fit for each scenario, however for the purposes here, it is adequate to show that there is larger data variability.

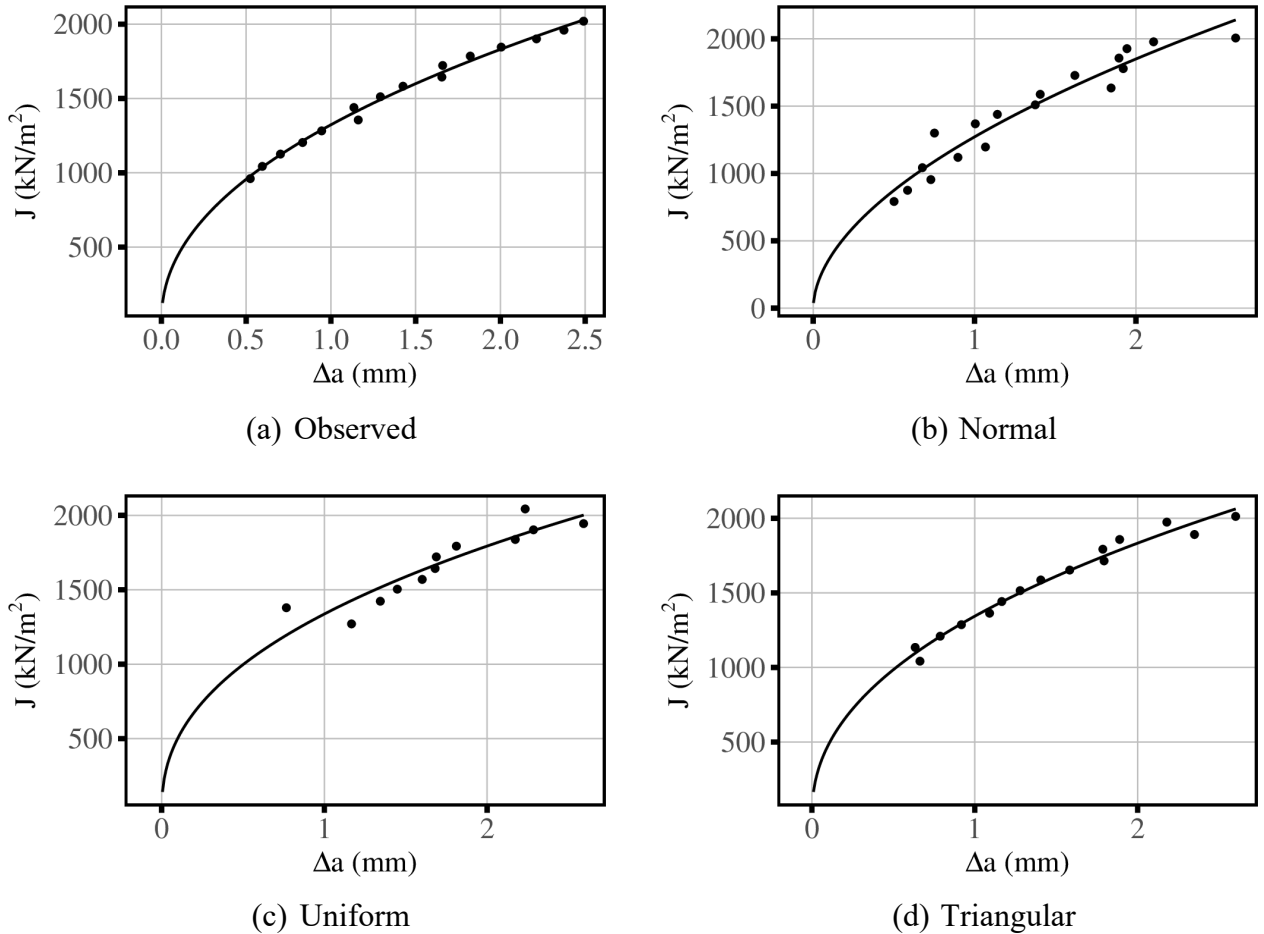


Figure 8. Data and fitted  $J$ - $R$  curves for (a) observed  $J$ - $R$  method data and for (b)-(d) simulated data for three candidate distributions based on the measurement tolerances specified in Table 1 and Table 6.

## 6. Monte Carlo Results

Monte Carlo simulations are performed by starting with the observed data, generating simulated data sets, and performing all the calculations to obtain 10,000 CTOD-R or  $J$ - $R$  curves for each combination of method and distribution (normal, uniform, and triangular). Some trials are disregarded if intermediate calculations failed to produce the minimum number of points needed to estimate  $a_{0q}$  or some other calculation error occurred (for example one of the nonlinear least squares fits did not converge, something that happens occasionally for no clear reason). A second set of simulations are also performed where the measurement tolerances specified in Table 1 and Table 6 are reduced by half. This will

elucidate potential benefits of improving the measurement process or revisiting the allowed tolerances in the methods and standards to match current measurement capabilities.

The output of the Monte Carlo simulations are 10,000 parameter estimates (alpha and eta pairs) each of which defines one possible CTOD-R or *J*-R curve. Since the curves themselves are important outputs for MOOSE, some kind of coverage bound around the observed data curve is an important secondary output. There are two common ways of treating a coverage bound around a curve (as opposed to an uncertainty for a parameter estimate), with different interpretations. The first is a “simultaneous” coverage band, where over all the *x*-values the entire observed curve *f*(*x*) falls within the upper and lower limits of the band with a specified probability (usually 95 %). The second is a “point-wise” coverage band, where at each *x*-value *x*<sub>*i*</sub>, the corresponding *f*(*x*<sub>*i*</sub>) value lies between the upper and lower limit of the band with a specified probability (usually 95 %). The point-wise approach does not make any claims about containing the entire *f*(*x*) curve with some probability but is commonly used and computationally simpler. The point-wise approach is used here, and to construct the point-wise coverage bounds on the CTOD-R and *J*-R curves as shown in Sec. 6.1 and Sec. 6.2, the process is as follows. For a given  $\Delta a$  value, method, and distribution, compute the 10,000 corresponding CTOD or *J* values from the 10,000 parameter pairs. The coverage interval, at that  $\Delta a$  value, is then the 0.025 and 0.975 quantiles of those 10,000 CTOD or *J* values. Repeating this step over the whole range of  $\Delta a$  values gives a smooth curve for both the 0.025 and 0.975 quantiles and thus 95 % coverage bounds around the CTOD-R or *J*-R curve from the observed data.

Table 7 shows the observed parameter estimates as well as the mean and standard deviations for  $a_{0q}$  and the two estimated parameters for the CTOD-R or *J*-R curves. Standard uncertainties are shown in parentheses next to the mean values.

Table 7. Resulting  $a_{0q}$  and power law fitting coefficients for the two methods and different data distributions.

Method	Distribution	$a_{0q}$	$\alpha$	$\eta$
CTOD-R	Observed	7.133	1.167	0.670
	Uniform	7.110 (0.138)	1.201 (0.136)	0.608 (0.101)
	Normal	7.117 (0.118)	1.189 (0.115)	0.628 (0.086)
	Triangular	7.126 (0.098)	1.181 (0.094)	0.644 (0.071)
<i>J</i> -R	Observed	7.014	1322.972	0.468
	Uniform	7.010 (0.034)	1325.153 (45.532)	0.453 (0.050)
	Normal	7.012 (0.026)	1321.996 (37.835)	0.460 (0.043)
	Triangular	7.013 (0.019)	1319.234 (29.833)	0.467 (0.035)

### 6.1. CTOD-R Results

Figure 9 shows results with a lower limit of 0.5 mm for the CTOD-R method. Each row of plots compares results by distribution when the measurement tolerances used in the simulations are reduced by half.

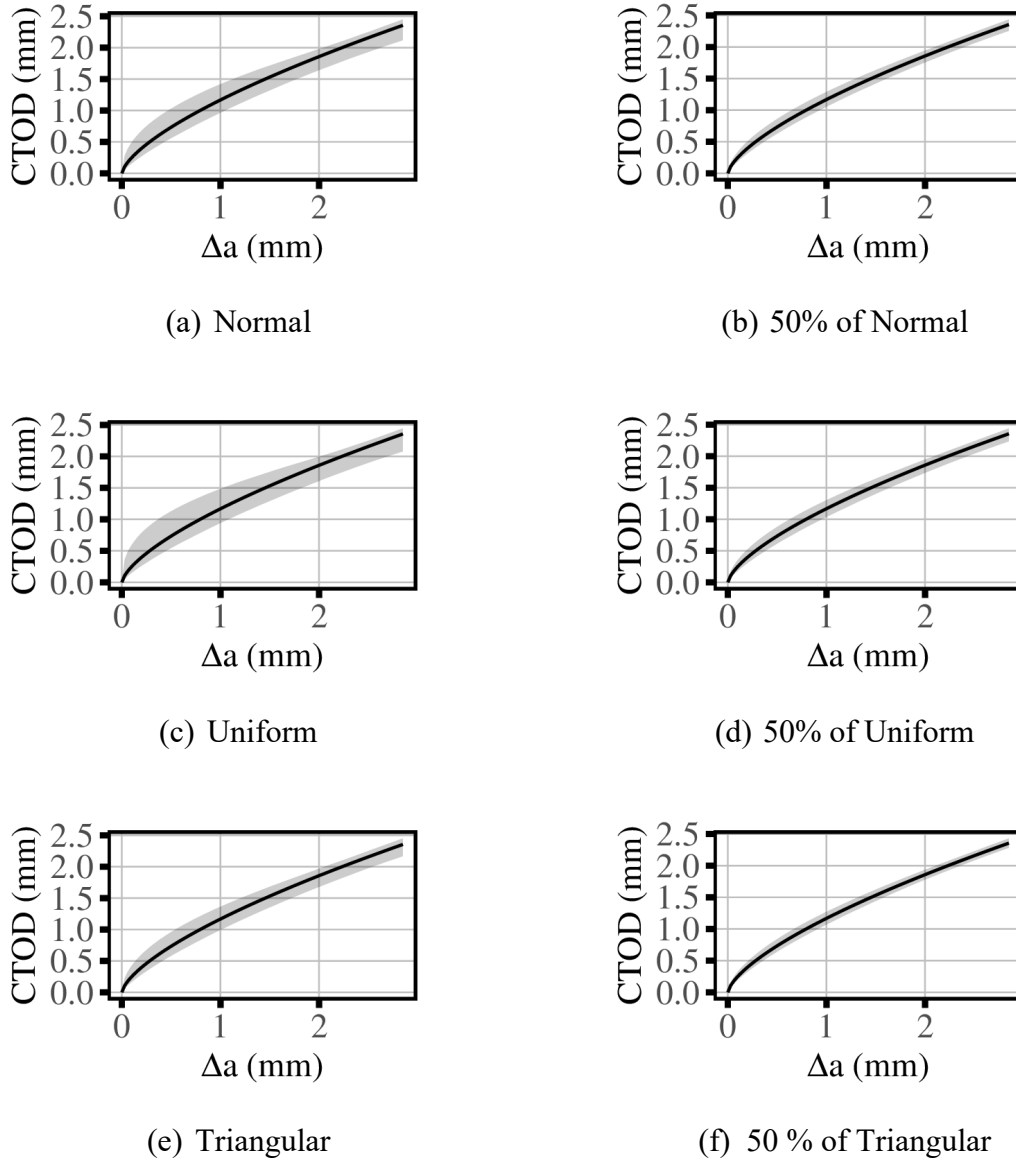


Figure 9. Estimated CTOD-R curves for observed data (black lines) and 95 % coverage bands estimated via simulation (gray shaded regions); (a)-(b) simulations with a normal distribution based on the full tolerance and on 50 % of the measurement tolerances specified in Table 1 and Table 6, (c)-(d) for a uniform distribution, (e)-(f) for a triangular distribution.

## 6.2. J-R Results

For the *J-R* method, Fig. 10 shows results with a lower limit of 0.5 mm. The top row shows results by distribution when the measurement tolerances used in the simulations are reduced by half, while the bottom row shows results when full measurement tolerances are used.

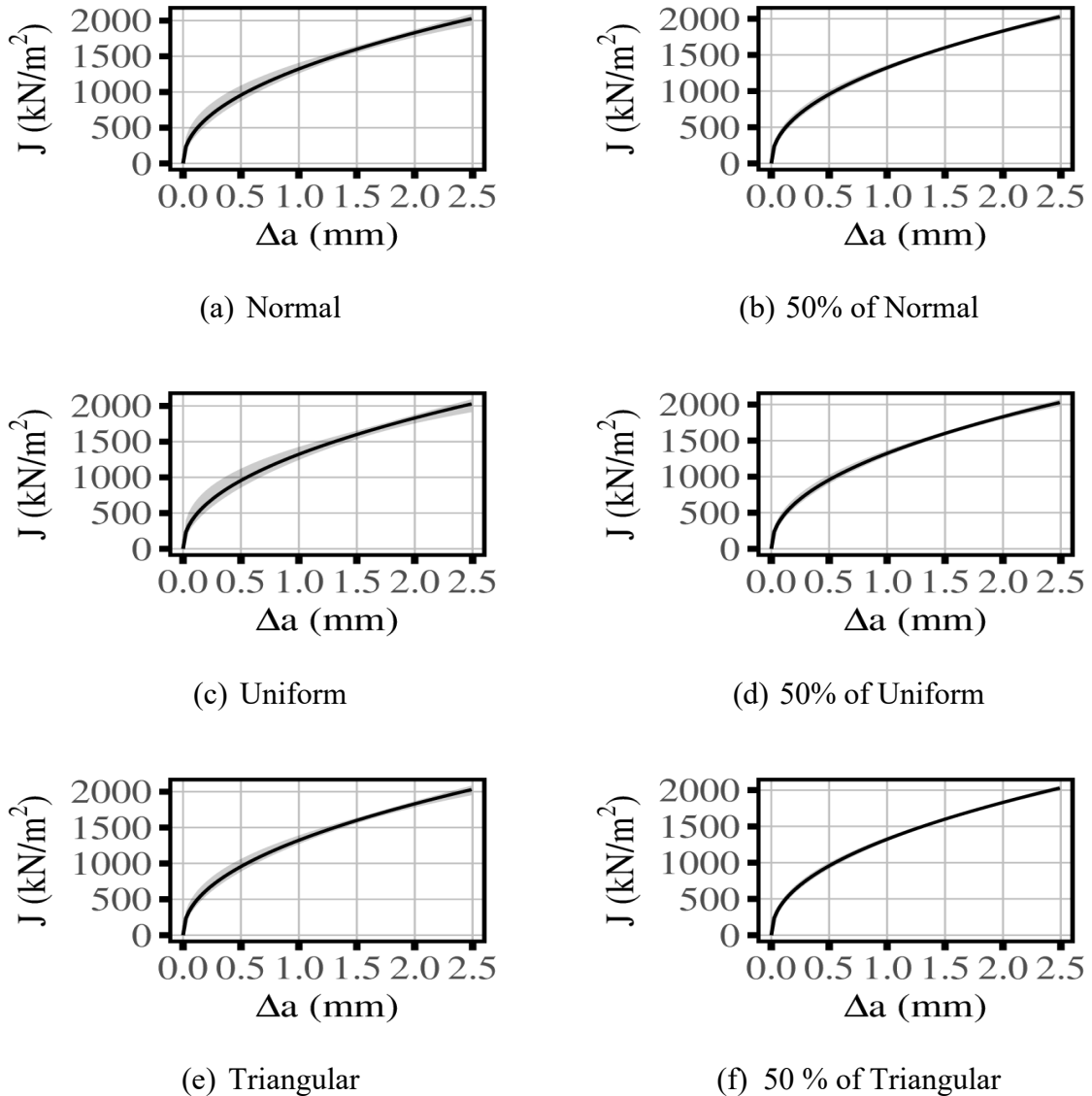


Figure 10. Estimated *J-R* curves for observed data (black lines) and 95 % coverage bands estimated via simulation (gray shaded regions). (a)-(b) simulations with a normal distribution based on the full tolerance and on 50 % of the measurement tolerances specified in Table 1 and Table 6, (c)-(d) for a uniform distribution, (e)-(f) for a triangular distribution.

## 7. Discussion

From the results presented in Fig. 9 and Fig. 10, an assumed uniform distribution of the added noise has the largest effect and leads to the widest coverage bands on the CTOD-R and J-R curves. Assuming the normal distribution (with standard deviation of half the specified tolerance) instead leads to much narrower coverage bands, and this effect is even more pronounced with the triangular distribution. Both the uniform and triangular distributions have hard limits on their possible values, whereas for the normal distribution no such hard boundary is present. Thus, for the normal distribution, although most of the values (about 95 % of them) will fall within  $\pm 2$  standard deviations, more extreme values can and will be sampled. Whether this representation of the measurement tolerances is accurate or not is an open question. For all three distributions considered, however, halving the uncertainty budget leads to a substantial reduction in the width of the coverage bands. A sensitivity study (easily supported by this Monte Carlo approach) that examines the contribution of individual uncertainty components to the uncertainty estimates could be a valuable source of information to illuminate where attention is best focused to improve measurements.

Comparing the coverage bands between the two methods is valuable even if they do not represent an accurate quantification of the uncertainty. The CTOD-R method is computationally simpler than the J-R method. However, the CTOD-R method includes one additional measurement tolerance and so it remains to be seen if the additional measurement tolerance influences the uncertainty more than the computational rigor with unknown uncertainties associated with fitting coefficients derived from finite element analysis (FEA) [10, 11]. While a sensitivity study is an important item to explore, a sensitivity study will not alter the conclusion that the J-R method has a smaller relative coverage band for every distribution and tolerance considered.

Another important finding from this work comes from the intermediate calculations. The measurement tolerances listed in Tables 1 and 6 produce simulated data sets that have much more variation than what is observed in the actual data for all assumed uncertainty distributions considered. This effect is so pronounced that it is difficult to even see the key features of each unloading. It is noteworthy that random uncertainties in physical measurements is expected to be significantly less than the measurement tolerance. What has been done thus far is to assume that the full measurement tolerance constitutes random noise. The measurement tolerance must include random signal noise but is expected to be dominated by non-linearities and bias. This study and presented method were devised to estimate the maximum uncertainty that can be expected from the test methods; refinements are part of the continuing work in this area.

There are several avenues for future work. First, the Monte Carlo approach used here fully supports sensitivity studies to investigate the contribution of individual uncertainty components to the final uncertainty estimates. Determining which distribution is appropriate for a particular measurand is also important. While the triangular distribution produces the smallest uncertainties, it may be the least relevant to the measurands required in these methods and therefore leads to an underestimated uncertainty.

Secondly, additional work is needed to investigate various fitting methods. Nonlinear least-squares regression was used to perform the fits required to obtain fracture toughness parameters; however, there are measurement errors associated with the independent variables (since they come from calculated values that are based on measurements that have errors), which is a clear violation of regression assumptions. Regression methods that account for errors in both independent and dependent variables, such as orthogonal distance regression or errors-in-variables regression, would technically be more appropriate for fitting. The current framework of the Monte Carlo simulation is flexible enough to determine if different fitting methods would improve upon the uncertainty, and if so, if that improvement warranted the additional computational rigor.

Lastly, this work focused on the original source documents for the test methods and significant research and improvements have been published since. New work using this method will include an examination of various suggested improvements to the measurements and analysis calculations.

## 8. Conclusions

This paper demonstrates that Monte Carlo methods can be successfully used to obtain the uncertainty of fracture toughness and fracture resistance curves. Monte Carlo simulations are an especially useful statistical tool when the measurement equation is too complex to estimate the uncertainty from propagation of errors. A detailed view of the computation process on the measured data to the resultant CTOD-R or  $J$ -R curve has also been shown. The final output of this work, the 95 % coverage bands around the CTOD-R and  $J$ -R curves, showed that the assumptions and choices surrounding the measurement tolerances play a large role in the size and shape of those coverage bands.

Much work remains before estimated standard uncertainties can be thoroughly evaluated for the single-edge-notched tension test, but this paper aims to foster discussion around these methods, specific assumptions, and the choices that support improvements in the test procedures, leading ultimately to a fully informed and robust consensus standard.

## References

- [1] International A (2020)– *ASTM E1820: Standard Test Method for Measurement of Fracture Toughness* (ASTM International West Conshohocken).  
<https://doi.org/10.1520/E0018-20>
- [2] Laboratory CMT (2010) Recommended Practice: Fracture Toughness Testing Using SE(T) Samples with Fixed-grip Loading. (CANMETMaterials, Ottawa, Alberta: Canada), 2010-31 (TR).
- [3] Company EUR (2010)– *Measurement of Crack Tip Opening Displacement (CTOD) - Fracture Resistance Curves Using Single Edge-Notched Tension (SENT) Specimens* (ExxonMobil Upstream Research Company, Houston, TX: USA).
- [4] Veritas DN (2006) Fracture Control for Pipeline Installation Methods Introducing Cyclic Plastic Strain. *Recommended Practice DNV-rp-f108*.
- [5] Institution BS (2014)– *BS-8571: Method of Test for Determination of Fracture Toughness in Metallic Materials Using Single Edge Notched Tension (SENT) Specimens* (BSI, London : UK).
- [6] BIPM, IFCC, IUPAC, OIML (2008) Guide to Expression of Uncertainty in Measurement. *Geneva: International Organization for Standardization; JCGM 100*.
- [7] BIPM, IFCC, ISO, IUPAC, IUPAP, OIML (2008) Evaluation of Measurement Data - Supplement 1 to the Guide to Expression of Uncertainty in Measurement - Propagation of Distributions Using a Monte Carlo Method. *Geneva: International Organization for Standardization; JCGM 102*.
- [8] Weeks TS , Lucon E (2014) Direct comparison of single-specimen clamped SE (T) test methods on X100 line pipe steel. *International Pipeline Conference*, (American Society of Mechanical Engineers), p V004T011A021.
- [9] Team RC (2013) R: A language and environment for statistical computing.
- [10] Tang H, Macia M, Minnaar K, Gioielli P, Kibey S, Fairchild D (2010) Development of the SENT Test for Strain-Based Design of Welded Pipelines. *2010 8th International Pipeline Conference*, pp 303-312. <https://doi.org/10.1115/ipc2010-31590>
- [11] Shen G, Gianetto JA, Tyson WR (2009) Measurement of JR curves using single-specimen technique on clamped SE (T) specimens. *The nineteenth international offshore and polar engineering conference*, (OnePetro).